

Effects of intrinsic AGN variability on optical QPOs related to sub-pc binary black hole systems in broad line AGN

XUEGUANG ZHANG^{*1}

¹Guangxi Key Laboratory for Relativistic Astrophysics, School of Physical Science and Technology, Guangxi University, Nanning, 530004, P. R. China

(Accepted March 14, 2025, ApJ)

ABSTRACT

In this manuscript, an oversimplified model is proposed to test the effects of intrinsic AGN variability on expected optical quasi-periodic oscillations (QPOs) related to sub-pc binary black hole systems (BBHs) in broad line AGN. The commonly accepted CAR (Continuous AutoRegressive) process is applied to describe intrinsic AGN variability related to each BH accreting system in a sub-pc BBH system. Considering obscurations related to orbital rotations with periodicity T_p , artificial light curves including signals for optical QPOs can be built. Then, comparing the intrinsic periodicities T_p with the measured robust periodicities T_o through the artificial light curves, distributions of T_p/T_o have four significant peaks around 1, 2, 3 and 4, leading less than half of the artificial light curves to have consistency between T_o and T_p . Moreover, different collected model parameters have few effects on the distributions of T_p/T_o , indicating the effects of intrinsic AGN variability on optical QPOs are significantly strong and stable. Furthermore, after checking properties of optical QPOs in the light curves with different time steps, there are tiny effects of time steps on optical QPOs.

Keywords: galaxies:active - galaxies:nuclei - quasars: supermassive black holes

1. INTRODUCTION

Sub-pc binary black hole systems (BBHs) are the preferred carriers on studying hierarchical formation and evolution of black holes. Due to observational technique limitations on spatially resolved photometric images, the long-standing optical quasi-periodic oscillations (QPOs) with periodicities around hundreds to thousands days have been accepted as good indicators for sub-pc BBHs in broad line active galactic nuclei (AGN). There are so far more than 200 candidates for sub-pc BBHs through implications of optical QPOs, such as the reported 1800days optical QPOs in PG 1302-102 in [Graham et al. \(2015a\)](#); [Kovacevic et al. \(2019\)](#), the 540days optical QPOs in PSO J334.2028+01.4075 in [Liu et al. \(2015\)](#), the optical QPOs in two samples of more than 160 optical QPOs in [Graham et al. \(2015\)](#); [Charisi et al. \(2016\)](#), the 1500days optical QPOs in SDSS J0159 in [Zheng et al. \(2016\)](#), the 1150days optical QPOs in Mrk915 in [Serafinelli et al. \(2020\)](#), the 1.2yr optical QPOs in Mrk231 in [Kovacevic et al. \(2020\)](#), the 1607days optical QPOs in SDSS J0252 in [Liao et al. \(2021\)](#), the 6.4yr optical QPOs in SDSS J0752 in [Zhang \(2022a\)](#), the 3.8yr optical QPOs in SDSS

J1321 in [Zhang \(2022b\)](#), the 340days optical QPOs in SDSS J1609 in [Zhang \(2023a\)](#), the 1000days optical QPOs in SDSS J1257 in [Zhang \(2023b\)](#) and the 550days optical QPOs in the known PG 1411+442 in [Zhang \(2025\)](#), etc. Here, the optical QPOs and the corresponding periodicities discussed in the manuscript are related to sub-pc BBH systems, not related to transient behavior ([Cui et al. 1998](#); [Wagoner et al. 2001](#); [Smith et al. 2018](#); [Goluchova et al. 2019](#)) arising in the accretion disk around single supermassive BH.

Although the optical QPOs can be well applied to detect sub-pc BBHs in broad line AGN, considering intrinsic AGN variability as one of the fundamental characteristics of AGN ([Ulrich et al. 1997](#); [Gezari et al. 2007](#); [Walsh et al. 2009](#); [Sanchez-Saez et al. 2019](#); [Zhang 2023c](#)), it is not clear for effects of intrinsic AGN variability on the detected optical QPOs in broad line AGN. Whether the effects of can lead to detected periodicities very different from the intrinsic values? To discuss the question is our main objective of this manuscript. Moreover, due to sub-pc BBHs as strongly preferred candidates for sources of nanohertz frequency gravitational waves as discussed in [Shannon et al. \(2015\)](#); [Taylor et al. \(2016\)](#); [Mingarelli et al. \(2017\)](#); [Sesana et al. \(2018\)](#); [Aggarwal et al. \(2019\)](#); [Arzoumanian et al. \(2023\)](#); [Charisi et al. \(2024\)](#), to report clear effects of intrinsic AGN variability on optical QPOs related to sub-pc BBHs in broad line AGN can provide

more confident results related to GWs produced by sub-pc BBHs.

It has been accepted that the CAR (Continuous AutoRegressive) process (Kelly, Bechtold & Siemiginowska 2009) and/or DRW (damped random walk) process (Kozłowski et al. 2010; Zu et al. 2013, 2016) can be applied to describe long-term intrinsic AGN variability (MacLeod et al. 2010). Certainly, as shown in MacLeod et al. (2010), there are about $\sim 2\%$ of the quasars of which light curves cannot be well described by the CAR process. Moreover, as discussed in Kelly et al. (2014); Kasliwal et al. (2017); Moreno et al. (2019); Yu et al. (2022); Kishore et al. (2024), rather than the simple CAR process, higher order CARMA(p , q) ($p \geq 1$ and $q \leq p$) (Continuous AutoRegressive Moving Average) process should be possibly preferred to describe AGN variability. However, considering the smaller number ratio $\sim 2\%$ of quasars of which light curves cannot be well described by the CAR process, and considering well-determined distributions of the CAR process parameters in common quasars variability but none-determined distributions of parameters in the CARMA process, the CAR process is accepted to widely describe intrinsic AGN variability. Meanwhile, considering the high quality light curves from the sky survey project of Zwicky Transient Facility (ZTF) (Bellm et al. 2019; Dekany et al. 2020), simulated light curves with similar time information from ZTF can be created by the CAR process. Therefore, combinations of obscurations due to orbital rotations as described in Section 2, effects of intrinsic AGN variability can be determined on expected optical QPOs related to sub-pc BBHs. This manuscript is organized as follows. Section 2 presents our model and main hypotheses, our main results and necessary discussions. Section 3 gives our main conclusions. And we have adopted the cosmological parameters of $H_0 = 70 \text{ km} \cdot \text{s}^{-1} \text{ Mpc}^{-1}$, $\Omega_\Lambda = 0.7$ and $\Omega_m = 0.3$ throughout this manuscript.

2. MAIN RESULTS AND NECESSARY DISCUSSIONS

2.1. Model and main hypotheses

In order to describe the expected periodic photometric variability properties of an assumed sub-pc BBH system by periodic variations of obscurations due to orbital rotations, the following three steps are applied in this manuscript.

First, totally accepted the CAR process discussed in Kelly, Bechtold & Siemiginowska (2009), two artificial long-term light curves (in photometric apparent magnitudes) $LC_{t,1}$ and $LC_{t,2}$ from two BH accreting systems in an assumed sub-pc BBH system can be created by

$$\begin{aligned} dLC_{t,1} &= \frac{-1}{\tau_1} LC_{t,1} dt + \sigma_{*,2} \sqrt{dt} \epsilon(t,1) + LC_{m1} \\ dLC_{t,2} &= \frac{-1}{\tau_2} LC_{t,2} dt + \sigma_{*,1} \sqrt{dt} \epsilon(t,2) + LC_{m2} \end{aligned} \quad (1)$$

Here, there are no considerations of any physical mechanisms on probable formations and/or evolutions of sub-pc BBHs, but only considering the simple point that two BH accreting systems in an assumed sub-pc BBH system can lead to two sources of photometric variability. Moreover, the main objective of the manuscript is to check effects of intrinsic AGN variability on expected optical QPOs related to sub-pc BBHs. Therefore, in an assumed sub-pc BBH system, we have accepted that each BH accreting system has its optical emission regions to be independent and complete. Otherwise, the mixed optical emission regions of the two BH accreting systems could not lead to expected optical QPOs. Therefore, the CAR process can be applied to trace the variability of the two BH accreting systems, and effects of sizes of accretion disks are not discussed any more in this manuscript. Furthermore, the BBHs on sub-pc scales harboring two individual BH accreting systems are mainly considered in the manuscript, not binary black hole systems embedded in the AGN gaseous disks as more recent discussions in Ishibashi & Grobner (2020); Fabj & Samsing (2024); Leong et al. (2025). In other words, considering the two BH accreting systems in sub-pc BBHs we mainly focused on have separated distance larger enough, even there were probable circumbinary disks around sub-pc BBH systems, there were few contributions of such circumbinary disks to optical emissions. Therefore, there are no further discussions on effects of probable circumbinary disks on our following results.

Here, considering high quality light curves from the ZTF, the time information t for the $LC_{t,1}$ and $LC_{t,2}$ are similar as the time information of SDSS quasars in ZTF. Here, the time information is collected from the ZTF g-band light curve of PG 1411+442 of which optical QPOs have been discussed in our more recent paper Zhang (2025), a known reverberation mapped broad line AGN in Kaspi et al. (2000); Peterson et al. (2004). Certainly, there are different time durations and different numbers of data points for different quasars in ZTF, however, there are few effects of time information on our final results, unless there are vary small number of data points in the ZTF light curve of the collected quasar.

Meanwhile, the two process parameters of intrinsic variability timescales τ_1 and τ_2 in the CAR process are randomly collected from 100days to 1000days, the common values in quasars as discussed in Kelly, Bechtold & Siemiginowska (2009); MacLeod et al. (2010). And, rather than giving values of σ_* , the parameters of $\frac{\tau_1 \times \sigma_{*,1}^2}{2}$ and $\frac{\tau_2 \times \sigma_{*,2}^2}{2}$ are randomly collected from 0.001 to 0.32, representing variances of $LC_{t,1}$ and $LC_{t,2}$. The values from 0.001 to 0.32 are the common values of variances of ZTF light curves of SDSS quasars. And the parameters of LC_{m1} and LC_{m2} , as mean apparent magnitudes of $LC_{t,1}$ and $LC_{t,2}$, are randomly collected from 16 to 19, common values for low redshift SDSS quasars.

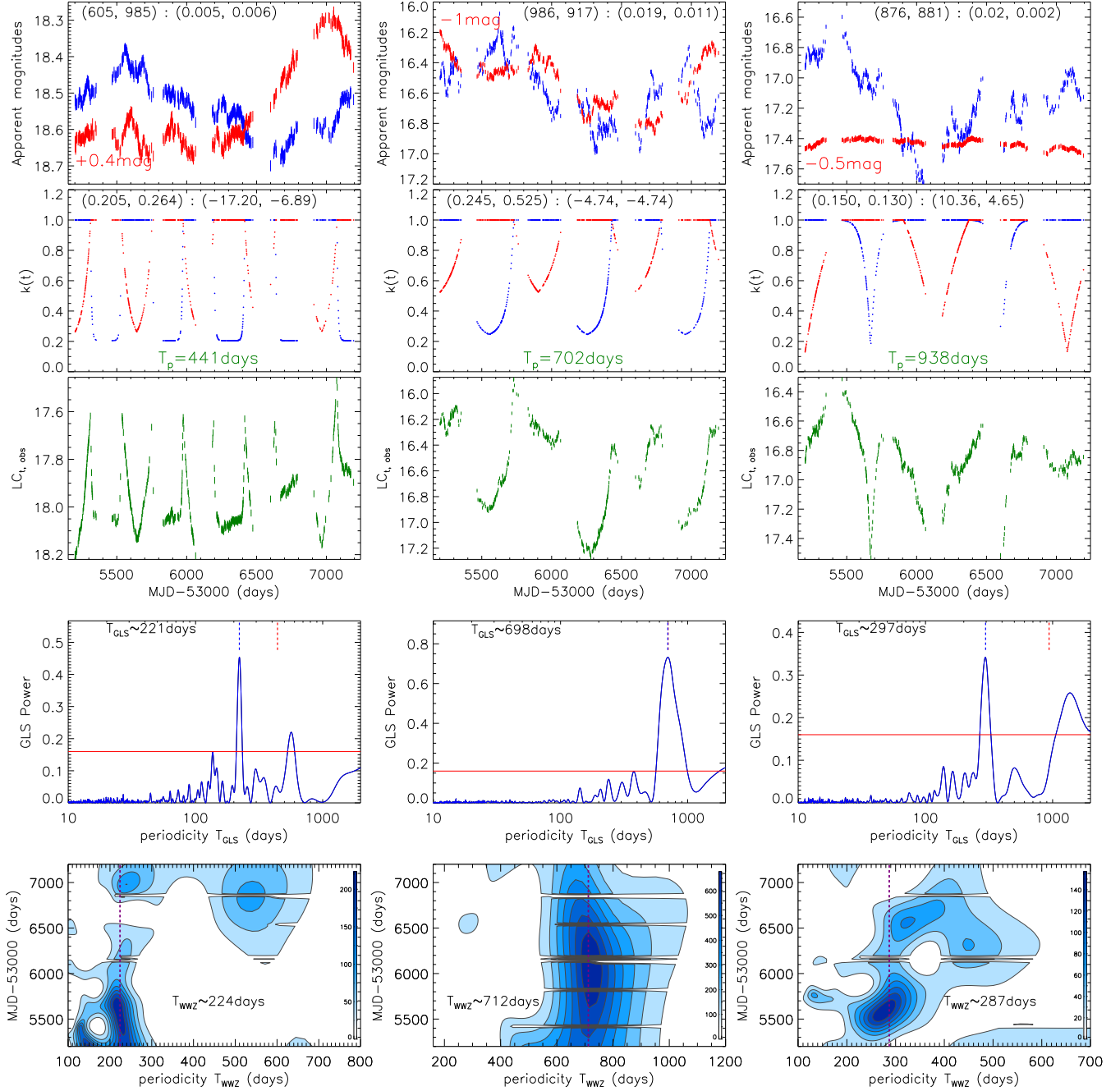


Figure 1. Top panels show the CAR process created $LC_{t,1}$ (in blue) and $LC_{t,2}$ (in red) by different process parameters of (τ_1, τ_2) (in units of days) : $(\sigma_{*,1}, \sigma_{*,2})$ (in units of $mag/days^{0.5}$) shown in the top region of each panel. The panels in the second row show the applied $k_1(t)$ (in blue) and $k_2(t)$ (in red) by different parameters of (k_{10}, k_{20}) : (α_1, α_2) shown in the top region of each panel and by different orbital periodicity T_p marked in dark green characters in bottom region of each panel. The panels in the third row show the determined $LC_{t,obs}$ after considering the obscurations due to orbital rotations. The panels in the fourth row show the GLS determined power properties of the corresponding $LC_{t,obs}$, with the horizontal red line marking the 5σ confidence levels based on white noise simulations. In each panel in the fourth row, the vertical dashed blue line marks the GLS determined periodicity $T_o (=T_{GLS})$, and the vertical dashed red line marks the position for the input T_p . The bottom panels show the WWZ determined two dimensional power properties of the corresponding $LC_{t,obs}$, with frequency step of 0.0001 and searching periodicities from 100 days to 2000 days. In each bottom panel, vertical dashed purple line marks the position of the WWZ determined periodicity T_{WWZ} which has been listed in the bottom region of each bottom panel. In each bottom panel, as the shown colorbar in the right hand, the contour levels in different colors show the numbers of data points in the evenly divided 1990×100 regions in the shown space of T_{WWZ} versus MJD-53000.

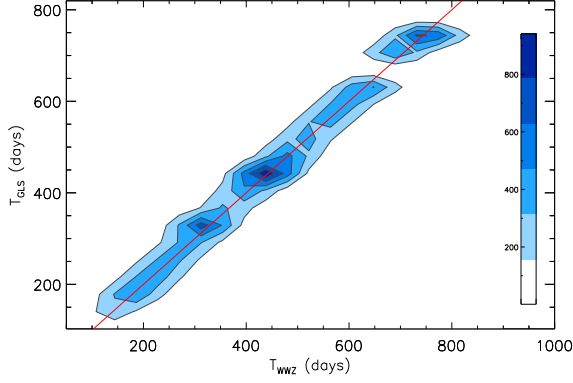


Figure 2. On the correlation between T_{GLS} and T_{WWZ} for the artificial light curves. The solid red line shows $T_{GLS} = T_{WWZ}$. As the shown colorbar in the right hand, the contour levels in different colors show the numbers of data points in the evenly divided 25×25 regions in the shown space of T_{WWZ} versus T_{GLS} .

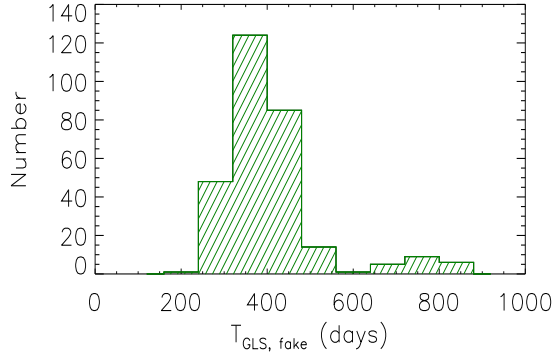


Figure 3. Distributions of the 293 $T_{GLS, fake}$ determined by applications of the GLS method in the 293 of the 100000 artificial light curves created by CAR process.

Moreover, based on the uncertainties $LC_{t, err, pg}$ of the ZTF g-band light curve $LC_{t, PG}$ of PG 1411+442, the uncertainties $LC_{t, err, 1}$ and $LC_{t, err, 2}$ of the $LC_{t, 1}$ and $LC_{t, 2}$ can be simply determined as

$$\frac{LC_{t, err, 1}}{LC_{t, 1}} = \frac{LC_{t, err, pg}}{LC_{t, PG}} = \frac{LC_{t, err, 2}}{LC_{t, 2}} \quad (2)$$

. Top panels of Fig. 1 shows three examples on $LC_{t, 1}$ and $LC_{t, 2}$ and the corresponding uncertainties.

Second, based on the created artificial light curves of $LC_{t, 1}$ and $LC_{t, 2}$, there are two periodic varying parameters $k_1(t)$ and $k_2(t)$ applied to trace obscurations due to orbital rotations with randomly selected periodicity T_p larger than 300days but smaller than 1000days, leading to the observed light curve $LC_{t, obs}$ as

$$10^{\frac{LC_{t, obs}}{-2.5}} = k_1(t) \times 10^{\frac{LC_{t, 1}}{-2.5}} + k_2(t) \times 10^{\frac{LC_{t, 2}}{-2.5}} \quad (3)$$

. Here, $k_1(t)$ and $k_2(t)$ with t within each cycle are created by piecewise functions as

$$k_1(t) = \begin{cases} 1 & (0 \leq \frac{t-t_0}{T_p} < \frac{1}{4}) \\ A_1 + B_1 t^{\alpha_1} & (\frac{1}{4} \leq \frac{t-t_0}{T_p} < \frac{1}{2}) \\ A_1 + B_1 (T_p - t)^{\alpha_1} & (\frac{1}{2} \leq \frac{t-t_0}{T_p} < \frac{3}{4}) \\ 1 & (\frac{3}{4} \leq \frac{t-t_0}{T_p} \leq 1) \end{cases} \quad (4)$$

$$k_2(t) = \begin{cases} A_2 + B_2 t^{\alpha_2} & (0 \leq \frac{t-t_0}{T_p} < \frac{1}{4}) \\ 1 & (\frac{1}{4} \leq \frac{t-t_0}{T_p} < \frac{1}{2}) \\ 1 & (\frac{1}{2} \leq \frac{t-t_0}{T_p} < \frac{3}{4}) \\ A_2 + B_2 (T_p - t)^{\alpha_2} & (\frac{3}{4} \leq \frac{t-t_0}{T_p} \leq 1) \end{cases} \quad (5)$$

Here, $k_1(t)$ and $k_2(t)$ have 1 as the maximum values, indicating none obscuration effects, and have $0 \leq k_{10} \leq 0.6$ and $0 \leq k_{20} \leq 0.6$ as the minimum values, indicating apparent obscuration effects due to orbital rotations. And $k_{10} = 0$ and $k_{10} > 0$ ($k_{20} = 0$ and $k_{20} > 0$) mean totally obscured and partly obscured. Simple discussions on different upper boundaries of minimum values of k_{10} and k_{20} from 0.6 can be found in the following subsection. And due to the time duration about 2000days of the artificial light curves, the selected periodicity is not larger than 1000days, to confirm the time durations at least two times larger than the periodicity, and the selected periodicity is not smaller than 300days after considering the minimum periodicity about 300days in the sample of QPOs in Graham et al. (2015). Once the input parameters k_{10} , α_1 , k_{20} , α_2 and the input periodicity T_p are clearly given, then the factors of A and B listed in the equation (4) and equation (5) can be clearly determined. The panels in the second row of Fig. 1 show three examples of $k_1(t)$ and $k_2(t)$ applied to the light curves shown in the top panels of Fig. 1, and the corresponding observed light curve $LC_{t, obs}$ after considering the orbital rotations expected obscurations traced by $k_1(t)$ and $k_2(t)$. Actually, different values of α_1 from α_2 and k_{10} from k_{20} can be reasonably accepted due to probably different properties of physical and geometric structures of the central two BH accreting systems.

Here, we should note that the periodic variations of obscuration is the key role leading to expected optical QPOs in an assumed sub-pc BBH system. However, it is hard to build an efficient model, not only considering physical properties of the materials for obscurations but also considering spatial properties of the materials. Therefore, we proposed the piecewise functions, equation (4) and equation (5), which can be applied to simply describe periodic variations of the obscurations expected by an assumed sub-pc BBH system. The different values of α_1 and α_2 can be applied to describe the corresponding properties of obscurations related to different properties of materials for obscurations. Meanwhile,

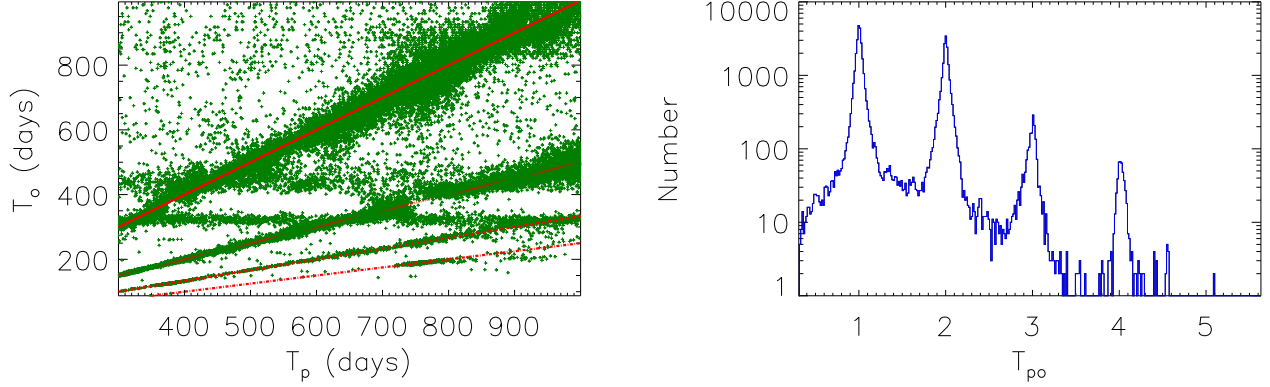


Figure 4. Left panel shows the correlation between the input periodicity T_p and the measured periodicity T_o from the $LC_{t, obs}$ including obscurations due to orbital rotations. Solid red line, dotted red line, dashed red line and dot-dashed red line show $T_p = T_o$, $T_p = 2 \times T_o$, $T_p = 3 \times T_o$ and $T_p = 4 \times T_o$, respectively. Right panel shows the distribution of T_{po} (ratio of T_p to T_o). In right panel, in order to show clearer features of the distribution, the plot in y-axis is shown in logarithmic coordinate.

for an assumed sub-pc BBH system, it is necessary to consider inclination of the orbit with respect to the line of sight. The inclination could lead to one BH accreting system only partly obscured by the other BH accreting system, indicating larger values of k_{10} and k_{20} applied in the piecewise functions. Therefore, different values of k_{10} , α_1 and k_{20} , α_2 can be applied to simply consider the effects of materials source for the obscurations and also the effects of inclination of the orbit.

Third, for each artificial light curve $LC_{t, obs}$, the widely accepted generalized Lomb-Scargle (GLS) method (Lomb 1976; Scargle 1982; Zechmeister & Kurster 2009; VanderPlas 2018) is applied to check periodicity. The panels in the fourth row of Fig. 1 show the GLS method determined power properties for the corresponding $LC_{t, obs}$ shown in the panels in the third row of Fig. 1. Meanwhile, in order to test robustness of the detected periodicity by the GLS method, the known WWZ (Weighted wavelet z-transform) technique (Foster 1996; An et al. 2016; Gupta et al. 2018; Kushwaha et al. 2020) has been applied to re-determine the periodicity in each artificial light curve, similar as what we have recently done in Zhang (2023a, 2025). The bottom panels of Fig. 2 shows the determined two-dimensional WWZ power properties for the artificial light curves shown in the panels in the third row of the Fig. 1, leading to the WWZ determined periodicity T_{WWZ} consistent with the GLS determined periodicity T_{GLS} in the three shown artificial light curves as examples.

Therefore, a simple procedure can be applied to create artificial light curves $LC_{t, obs}$ including apparent obscurations due to orbital rotations, based on the three steps above including 11 parameters, the CAR process parameters of τ_1 , τ_2 , $\sigma_{*,1}$, $\sigma_{*,2}$, mean magnitudes LC_{m1} and LC_{m2} of light curves $LC_{t, 1}$ and $LC_{t, 2}$, minimum values of k_{10} and k_{20} , input pe-

riodicity T_p , power indices of α_1 and α_2 . Finally, based on the randomly selected 11 parameters, 50000 artificial light curves $LC_{t, obs}$ are created, and the corresponding periodicities T_{GLS} and T_{WWZ} are determined by the GLS method and the WWZ technique.

Before ending the section, three additional points are noted. First and foremost, Fig. 2 shows the correlation between the determined periodicity T_{GLS} by the GLS method and the determined periodicity T_{WWZ} by the WWZ technique for the artificial light curves. There is a strong linear correlation between T_{GLS} and T_{WWZ} with Spearman Rank correlation coefficient about 0.91 ($P_{null} < 10^{-10}$), and with the mean value of T_{GLS}/T_{WWZ} about 0.998 ± 0.081 (the mean value plus/minus the standard deviation). The results in Fig. 2 strongly indicate that the measured periodicities in the artificial light curves to be robust enough. After considering the linear correlation between T_{GLS} and T_{WWZ} , the GLS determined periodicities T_{GLS} are accepted as the measured periodicity T_o in the artificial light curves. Actually, applications of T_{WWZ} as T_o can lead to the similar final results.

Besides, we do focus on the expected optical QPOs after main considerations of obscurations due to orbital rotations which can be described by piecewise functions described by equation (3), equation (4) and equation(5), not on the subtle spatial structures. In other words, rather than applications of physical mechanisms, a mathematics-oriented approach is applied, leading to the similar photometric variability properties expected by the physical mechanism related to the sub-pc BBHs.

Last but not the least, although the mathematics-oriented approach above can lead to expected optical QPOs, it is also necessary to check the probability of optical QPOs actually from intrinsic AGN variability, i.e., to check the effects of red nosies on the detected QPOs. Here, similar as what we have

recently done in Zhang (2023a, 2025) and similar as discussed results in Vaughan et al. (2016), fake QPOs related to red noises can be checked in the 100000 artificial light curves (50000 $LC_{t,1}$ and 50000 $LC_{t,2}$) which have been created by equation (1) above. Accepted the simple criterion that there is significant peak within the range from 100days to 1000days in the GLS power above the 5σ confidence level through white noise simulations, QPOs with GLS method determined periodicities $T_{GLS, fake}$ can be detected in 293 of the 100000 artificial light curves, leading to the probability¹ about $293/100000 = 2.93 \times 10^{-3}$ for detected fake QPOs related to red noises. Distribution of the 293 $T_{GLS, fake}$ is shown in Fig. 3. Therefore, there are few effects of red noises on detecting QPOs. Moreover, in the procedure above, pointed periodic variations of obscurations can apparently lead to expected periodic signals in the artificial light curves $LC_{t, obs}$, thus only simple discussions above on effects of red noises are given, and there are no further discussions on effects of red noises.

2.2. Main Results

It is necessary to check whether are there the consistency between the input periodicity T_p and the measured periodicity T_o for the artificial light curves. Left panel of Fig. 4 shows the correlation between T_p and T_o for the 50000 $LC_{t, obs}$. Right panel of Fig. 4 shows the distribution of the ratio T_{po} of T_p to T_o . It is clear that part of the artificial light curves $LC_{t, obs}$ have the measured periodicity T_o to be two to four times smaller than the input periodicity T_p . Meanwhile, as the shown examples in Fig. 1, the corresponding T_{po} can be found as $T_{po} \sim 1.99$, $T_{po} \sim 1.01$ and $T_{po} \sim 3.2$, respectively. And among the 50000 $LC_{t, obs}$, there are $N_{po1} = 29240$, $N_{po2} = 18336$, $N_{po3} = 1901$ and $N_{po4} = 523$ as the numbers of $LC_{t, obs}$ with $T_{po} \leq 1.5$, with $1.5 \leq T_{po} \leq 2.5$, with $2.5 \leq T_{po} \leq 3.5$ and with $T_{po} \geq 3.5$. The number ratios are about $N_p = N_{po1} : N_{po2} : N_{po3} : N_{po4} \sim 56 : 35 : 3.6 : 1$. Therefore, about 41.52% ($(N_{po2} + N_{po3} + N_{po4})/50000$) of the 50000 $LC_{t, obs}$ have the measured periodicity T_o very smaller (at least two times smaller) than the input periodicity T_p , due to the expected apparent effects of intrinsic AGN variability. In detail, about 36.67% ($N_{po2}/50000$), 3.8% ($N_{po3}/50000$) and 1.05% ($N_{po4}/50000$) of the 50000 $LC_{t, obs}$ have the measured periodicity T_o about two times smaller, three times smaller and at least four times smaller than the input periodicity T_p , respectively. Here, through the linear correlations shown in the left panel of Fig. 4, the GLS determined periodicity can be reasonably accepted as the measured periodicity

T_o of the QPOs in the simulated $LC_{t, obs}$ with few effects of red noises, otherwise there were no correlations between the measured T_o and the input T_p .

Moreover, it is necessary to check probable effects of the collected model parameters on the T_{po} . Here, for the parameter pairs $[\tau_1, \tau_2]$, $[\sigma_{*,1}, \sigma_{*,2}]$, $[LC_{m1}, LC_{m2}]$, $[k_{10}, k_{20}]$ and $[\alpha_1, \alpha_2]$ for the $LC_{t, 1}$ and $LC_{t, 2}$, distributions of T_{po} are compared for the $LC_{t, obs}$ with the absolute difference between each parameter pair larger than or smaller than the mean value of the absolute difference, such as the compared results between the $LC_{t, obs}$ with $|\tau_1 - \tau_2| < 300days$ (300days as the mean value of $|\tau_1 - \tau_2|$ for all the 50000 $LC_{t, obs}$) and the $LC_{t, obs}$ with $|\tau_1 - \tau_2| > 300days$. The compared distributions of T_{po} are shown in Fig. 5, and there are not different distributions of T_{po} , indicating few effects of the collected model parameters on the shown results in the right panel of Fig. 4.

Furthermore, based on the 50000 artificial light curves created above, the following procedures are done to check effects of different time steps of light curves on our final results. Based on each artificial light curve, three additional light curves LC_{43} , LC_{42} , LC_{31} are created through 3/4, 2/4 and 1/3 of the data points randomly collected. And the GLS method is applied to determine the periodicities T_{p43} , T_{p42} and T_{p31} in the three additional light curves. Then, distributions of ratios of $T_{43} = T_o/T_{p43}$ (mean value 1.009), $T_{42} = T_o/T_{p42}$ (mean value 1.016) and $T_{31} = T_o/T_{p31}$ (mean value 1.029) are shown in Fig. 6 for the $LC_{t, obs}$ and the corresponding additional light curves LC_{43} , LC_{42} , LC_{31} . There are 97.3% of the LC_{43} having $0.9 < T_{43} < 1.1$, 95.1% of the LC_{43} having $0.9 < T_{42} < 1.1$, and 92.9% of the LC_{31} having $0.9 < T_{31} < 1.1$. Therefore, there are slight effects of different time steps of the light curves on the final determined periodicities. Meanwhile, considering the mean values with $T_{43} < T_{42} < T_{31}$, larger time steps of a light curve should lead to smaller measured periodicity.

Before ending the subsection, the following four additional points are discussed. First, besides the 50000 artificial light curves created above, 50000 another light curves are created with the same values of $\alpha_1 = \alpha_2$, and 50000 another light curves are created with the same values of $k_{10} = k_{20} = 0$, and 50000 another light curves are created with the time durations very different from those applied above based on light curves of the other quasars from the ZTF. Then, based on the re-created light curves, similar results can be confirmed as the results shown in Fig. 4 and in Fig. 5 and in Fig. 6, to support that the collected values of α and k_0 and different time durations having few effects on our final results, probably indirectly indicating central geometric structures having similar effects on obscurations due to orbital rotations related to sub-pc BBHs. Second, upper boundaries k_{u10} and k_{u20} of minimum values of $k_{10} < k_{u10}$ and $k_{20} < k_{u20}$ have been col-

¹ The probability is about 6 times larger than the probability 4.8×10^{-4} in Zhang (2025). However, considering that there are no restrictions on CAR parameters no restrictions on range of periodicity, the larger probability can be reasonably accepted.

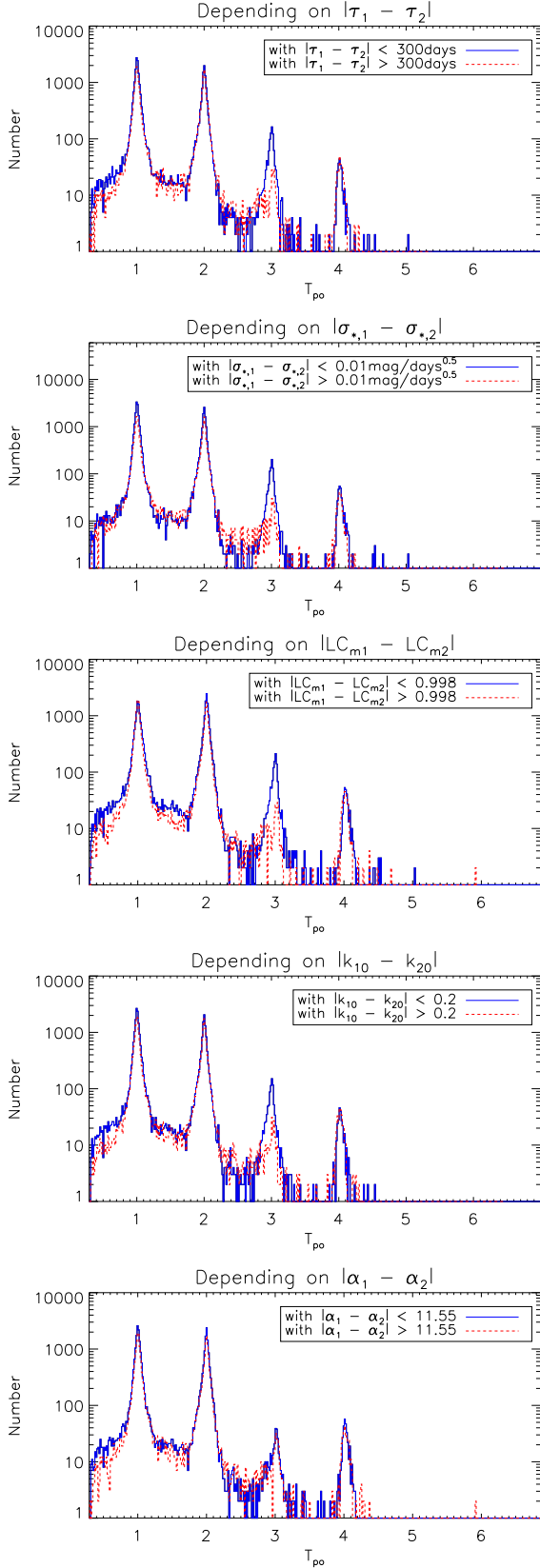


Figure 5. In each panel, distributions of T_{po} are compared for the $LC_{t,obs}$ with the different ranges of the difference of the model parameter pairs. The applied model parameter pair are listed in title of each panel, the mean value of the difference of the model parameter pair is marked in top right region of each panel.

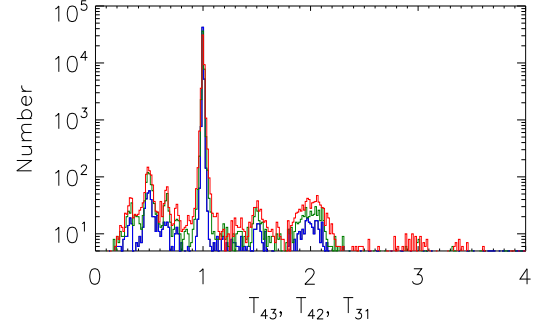


Figure 6. Distributions of T_{43} (in blue), T_{42} (in dark green) and T_{31} (in red) of the 50000 artificial light curves $LC_{t,obs}$ and the corresponding additional light curves LC_{43} , LC_{42} , LC_{31} .

lected to be larger than 0.6, leading to part of artificial light curves have the measured periodicities T_p with confidence levels smaller than 5σ , due to weaker obscurations due to orbital rotations. However, after removing the weaker QPOs, the similar results can be confirmed as the results shown in Fig. 4 and in Fig. 5 and in Fig. 6, not providing clues to change the effects of intrinsic AGN variability on optical QPOs. Third, as discussed above, intrinsic AGN variability have apparent and stable effects on optical QPOs, indicating there could be probably different periodicities in light curves in different epochs for one assumed sub-pc BBH. Although we cannot clearly find the key role to control the variability of the periodicities in different epochs, the results could be applied to explain why there were weaker evidence for the periodicity in the known PG 1302-102 if the ASAS-SN (All-Sky Automated Survey for SuperNovae) data were combined with the previous LINEAR+CRTS (Lincoln Near-Earth Asteroid Research, Catalina Real-time Transient Survey) data discussed in Liu et al. (2018), due to probably different measured periodicity in the light curves from the ASAS-SN.

2.3. further discussions

As discussed above, the time information of the ZTF g-band light curve of PG 1411+442 is applied to create the simulated light curves, it is necessary to check whether different time information can lead to the same final results. Here, light curves of another ten randomly collected SDSS quasars have been collected from ZTF (g-band), and the corresponding time information are accepted to create the simulated light curves through the same procedures above. And then, totally similar results can be confirmed that about 40%-45% ($(N_{po2} + N_{po3} + N_{po4})/50000$) of the 50000 $LC_{t,obs}$ have the measured periodicity T_o very smaller (at least two times smaller) than the input periodicity T_p , due to the expected apparent effects of intrinsic AGN variability. Table 1 lists the basic information of the light curves and the corresponding results on the simulated results based on the time information

of the ZTF light curves of the ten collected SDSS quasars. Here, besides the listed results in Table 1, there are no plots on the results, due to totally similar as the ones shown in Fig. 4.

Moreover, based on the time information of the ZTF g-band light curves of the collected 10 SDSS quasars, similar procedures have been done to check effects of different time steps of the light curves on the final determined periodicities, through checking properties of additional light curves LC_{43} , LC_{42} , LC_{31} created through 3/4, 2/4 and 1/3 of the data points randomly collected through the artificial light curves. As the shown results on the mean values of the corresponding T_{43} , T_{42} and T_{31} in the last three columns in Table 1, it can be re-confirmed slight effects of different time steps of the light curves on the final determined periodicities. Here, besides the listed results on mean values of T_{43} , T_{42} and T_{31} in Table 1 based on the time information of the ZTF g-band light curves of the collected 10 SDSS quasars, there are no plots on distribution of T_{43} , T_{42} and T_{31} , due to totally similar as the ones shown in Fig. 6. Meanwhile, when additional light curves LC_{42} and LC_{31} are created through 2/4 and 1/3 of the data points randomly collected from the artificial light curves, the quality (the value of time duration divided by the number of data points) of the LC_{42} and LC_{31} should be similar as that of common light curves collected from the CSS (Catalina Sky survey) (Drake et al. 2009). Therefore, there are no further discussions on simulated results through time information of CSS light curves.

Furthermore, due to the discussions above on the sub-pc BBHs, it is interesting to check the probable beaming effects by probably relativistic orbital rotations on observational photometric properties. Based on discussed BBH model in Eracleous et al. (2012), the expected space separation of the central two BH accreting systems can be estimated as

$$S_{BBH} \sim 0.432M_8 \left(\frac{T_{qpo}}{2652M_8} \right)^{2/3} pc \quad (6)$$

with M_8 as the total BH mass in units of $10^8 M_\odot$ and T_{qpo} as the orbital periodicity in units of years. Meanwhile, assumed a simple circular orbital, the sum V of the absolute orbital velocities $|V_1|$ and $|V_2|$ of the two BHs can be expected as

$$\begin{aligned} V &= |V_1| + |V_2| = \sqrt{\frac{GM_8}{S_{BBH}}} \\ &= 13814 \text{km/s} \times \left(\frac{M_8}{T_{qpo}} \right)^{1/3} \end{aligned} \quad (7)$$

with G as the gravitational constant. After simply considering $M_8 \sim 10$ and $T_{qpo} \sim 2.74$ years (mean values of the sub-pc BBH system candidates listed in Graham et al. 2015), the determined Lorentz factor is only about $\frac{1}{\sqrt{1-(V/c)^2}} \sim 1.0025$ (c as the light speed), indicating very weak beaming effects by

orbital rotation on the observational photometric properties. Therefore, there are no further discussions on beaming effects on our discussed results.

Before ending the section, we should note that the applied CAR process and the piecewise functions are not completely accurate but only mathematics-oriented approach for intrinsic AGN variability after considering the obscurations related to orbital motions in sub-pc BBH systems. Therefore, in order to test and confirm our results reported and discussed in this manuscript, it will be our objective in the near future to test whether are there different periodicities in different epochs from those of the optical QPOs reported in the literature.

3. MAIN SUMMARY AND CONCLUSIONS

Our main summary and conclusions are as follows.

- Considering intrinsic AGN variability described by the CAR process, combining with orbital rotations expected obscurations described by piecewise functions, effects of intrinsic AGN variability on optical QPOs related to sub-pc BBHs can be checked.
- The measured periodicities T_o are not well consistent with the input orbital periodicity T_p , only about 41.52% of the artificial light curves have $T_o \sim T_p$. However, about 36.67% of the artificial light curves have $T_o \sim T_p/2$, about 3.8% of the artificial light curves have $T_o \sim T_p/3$, and about 1.05% of the artificial light curves have $T_o < T_p/4$. After considering effects of the collected model parameters, total similar results can be confirmed, indicating strong and stable effects of the intrinsic AGN variability on optical QPOs.
- Moreover, based on the light curves with data points randomly collected from the artificial light curves, larger time steps of light curves have tiny effects on the measured optical periodicities, and can probably lead to a bit smaller measured optical periodicities.
- It will be our objective in the near future to check whether the reported optical QPOs in the literature should have different periodicities detected through light curves in different epochs from different sky survey projects.

ACKNOWLEDGMENTS

Zhang gratefully acknowledge the anonymous referee for giving us constructive comments and suggestions to greatly improve the paper. Zhang gratefully thanks the kind financial support from GuangXi University and the kind grant support from NSFC-12173020 and NSFC-12373014. This paper has made use of the data from the ZTF <https://www.ztf.caltech.edu>.

Table 1. Basic results through the collected ZTF light curves of the 10 SDSS quasars

obj	N	T_d	mag	N_{po1}	N_{po2}	N_{po3}	N_{po4}	N_p	T_{43}	T_{42}	T_{31}
PG 1411+442	532	1992	14.99±0.012	29240	18336	1901	523	55.9:35.1:3.63:1	1.009	1.016	1.029
J02:18:38.90-04:20:41.28	284	1678	18.41±0.044	28244	19522	1712	522	54.1:37.4:3.28:1	1.033	1.055	1.079
J04:37:21.57+12:58:31.43	220	1913	18.34±0.040	28250	19024	2113	613	46.1:31.1:3.45:1	1.036	1.059	1.083
J09:44:00.33+28:52:26.75	248	1890	18.00±0.034	30113	17697	1677	513	58.7:34.5:3.27:1	1.036	1.057	1.081
J10:10:44.49+00:43:31.08	200	1879	16.12±0.019	28490	18876	2051	583	48.9:32.4:3.52:1	1.037	1.063	1.084
J11:27:36.88+24:49:23.52	318	1915	17.44±0.022	29081	18460	1956	503	57.8:36.7:3.89:1	1.033	1.047	1.072
J12:06:48.31+06:59:12.12	361	1914	17.57±0.024	28931	18451	2045	573	50.5:32.2:3.57:1	1.029	1.039	1.074
J14:54:34.34+08:03:36.35	309	1922	16.75±0.018	27765	19251	2361	623	44.6:30.9:3.79:1	1.035	1.043	1.075
J16:27:50.54+47:36:23.39	393	1921	17.62±0.021	28787	18605	2047	561	51.3:33.2:3.65:1	1.022	1.041	1.058
J21:12:04.84-06:35:35.16	244	1865	17.76±0.029	28386	18921	2098	595	47.7:31.8:3.53:1	1.034	1.049	1.069
J21:23:47.83-08:28:42.60	216	1862	18.16±0.031	28476	18890	2048	586	48.6:32.2:3.49:1	1.038	1.066	1.079

Notes: The first column shows the name of the collected 10 SDSS quasars in the format of SDSS Jhh:mm:ss.ss±dd:mm:ss.ss, except the PG 1411+442. The second column and the third column show the number of data points and the time duration in the collected 1day binned ZTF g-band light curve of each quasar. The fourth column shows the mean magnitude and the mean uncertainty of the collected 1day binned ZTF g-band light curve of each quasar. The fifth to eighth column shows the determined N_{po1} , N_{po2} , N_{po3} , N_{po4} among the 50000 simulated light curves with the input time information from the collected 1day binned ZTF g-band light curve of each quasar. The ninth column shows the determined $N_p = N_{po1} : N_{po2} : N_{po3} : N_{po4}$. The last three columns show the determined mean values of $T_{43} = T_o/T_{p43}$, $T_{42} = T_o/T_{p42}$ and $T_{31} = T_o/T_{p31}$.

REFERENCES

- Aggarwal, K.; Arzoumanian, Z.; Baker, P. T.; et al., 2019, ApJ, 880, 116
- An, T.; Lu, X.; Wang, J., 2016, A&A, 585, 89
- Arzoumanian, Z.; Baker, P. T.; Blecha, L.; et al., 2023, ApJL, 951, 28
- Bellm, E. C.; Kulkarni, S. R.; Barlow, T.; et al., 2019, PASP, 131, 068003
- Charisi, M.; Bartos, I.; Haiman, Z.; et al., 2016, MNRAS, 463, 2145
- Charisi, M.; Taylor, S. R.; Witt, C. A.; Runnoe, J., 2024, PhRvL, 132, 061401
- Cui, W.; Zhang, S. N.; Chen, W., 1998, ApJL, 492, L53
- Dekany, R.; Smith, R. M.; Riddle, R.; et al., 2020, PASP, 132, 038001
- Drake, A. J.; Djorgovski, S. G.; Mahabal, A.; et al., 2009, ApJ, 696, 870
- Eracleous, M.; Boroson, T. A.; Halpern, J. P.; Liu, J., 2012, ApJS, 201, 23
- Fabj, G.; Samsing, J., 2024, MNRAS, 535, 3630
- Foster, G., 1996, AJ, 112, 1709
- Gezari, S.; Halpern, J. P.; Eracleous, M., 2007, ApJS, 169, 167
- Goluchova, K.; Torokl, G.; Sramkova, E.; Abramowicz, M. A.; Stuchlikl, Z.; Horak, J., 2019, A&A Letters, 622, L8
- Graham, M. J.; Djorgovski, S. G.; Stern, D.; et al., 2015a, Natur, 518, 74
- Graham, M. J.; Djorgovski, S. G.; Stern, D.; et al., 2015, MNRAS, 453, 1562
- Gupta, A. C.; Tripathi, A.; Wiita, P. J.; et al., 2018, A&A, 616, 6
- Ishibashi, W.; Grobner, M., 2020, A&A, 639, 108
- Kaspi, S.; Smith, P. S.; Netzer, H.; Maoz, D.; Jannuzi, B. T.; Giveon, U., 2000, ApJ, 533, 631
- Kasliwal, V. P.; Vogeley, M. S.; Richards, G. T., 2017, MNRAS, 470, 3027
- Kelly, B. C.; Bechtold, J.; Siemiginowska, A., 2009, ApJ, 698, 895
- Kelly, B. C.; Becker, A. C.; Sobolewska, M.; Siemiginowska, A.; Uttley, P., 2014, ApJ, 788, 33
- Kishore, S.; Gupta, A. C.; Wiita, P. G., 2024, ApJ, 960, 11
- Kovacevic, A. B.; Popovic, L. C.; Simic, S.; Ilic, D., 2019, ApJ, 871, 32
- Kovacevic, A. B.; Yi, T.; Dai, X.; et al., 2020, MNRAS, 494, 4069
- Kozlowski, S.; Kochanek, C. S.; Udalski, A., et al., 2010, ApJ, 708, 927
- Kushwaha, P.; Sarkar, A.; Gupta, Alok C.; Tripathi, A.; Wiita, P. J., 2020, MNRAS, 499, 653
- Leong, S. H. W.; Janquart, J.; Sharma, A. K.; Martens, P.; Ajith, P.; Hannuksela, O. A., 2025, ApJL, 979, L27
- Liao, W.; Chen, Y.; Liu, X.; et al., 2021, MNRAS, 500, 4025
- Liu, T.; Gezari, S.; Heinis, S.; et al., 2015, ApJL, 803, L16
- Liu, T.; Gezari, S.; Miller M. C., 2018, ApJL, 859, L12
- Lomb, N. R., 1976, Ap&SS, 39, 447
- MacLeod, C. L.; Ivezić, Z.; Kochanek, C. S.; et al., 2010, ApJ, 721, 1014
- Mingarelli, C. M. F.; Lazio, T. J. W.; Sesana, A.; et al., 2017, NatAs, 1, 886

- Moreno, J.; Vogeley, M. S.; Richards, G. T.; Yu, W., 2019, *PASP*, 131, 063001
- Peterson, B. M.; Ferrarese, L.; Gilbert, K. M.; et al., 2004, *ApJ*, 613, 682
- Serafinelli, R.; Severgnini, P.; Braitto, V.; et al., 2020, *ApJ*, 902, 10
- Sesana, A.; Haiman, Z.; Kocsis, B.; Kelley, L. Z., 2018, *ApJ*, 856, 42
- Sanchez-Saez, P.; Lira, P.; Cartier, R.; et al., 2019, *ApJS*, 242, 10
- Scargle, J. D., 1982, *ApJ*, 263, 835
- Shannon, R. M.; Ravi, V.; Lentati, L. T.; et al., 2015, *Sci*, 349, 1522
- Smith, K. L.; Mushotzky, R. F.; Boyd, P. T.; Wagoner, R. V., 2018, *ApJL*, 860, L10
- Taylor, S. R.; Huerta, E. A.; Gair, J. R.; McWilliams, S. T., 2016, *ApJ*, 817, 70
- Ulrich, M. H.; Maraschi, L.; Urry, C. M., 1997, *ARA&A*, 35, 445
- VanderPlas, J. T., 2018, *ApJS*, 236, 16
- Vaughan, S.; Uttley, P.; Markowitz, A. G.; et al., 2016, *MNRAS*, 461, 3145
- Walsh, J. L.; Minezaki, T.; Bentz, M. C.; et al., 2009, *ApJS*, 185, 156
- Wagoner, R. V.; Silbergleit, A. S.; Ortega-Rodriguez, M., 2001, *ApJL*, 559, L25
- Yu, W.; Richards, G. T.; Vogeley, M. S.; Moreno, J.; Graham, M. J., 2022, *ApJ*, 936, 132
- Zechmeister, M.; Kurster, M., 2009, *A&A*, 496, 577
- Zhang, X. G., 2022a, *MNRAS*, 512, 1003, arXiv:2202.11995
- Zhang, X. G., 2022b, *MNRAS*, 516, 3650, arXiv:2209.01923
- Zhang, X. G., 2023a, *MNRAS*, 526, 1588, arXiv:2309.08078
- Zhang, X. G., 2023b, *MNRAS*, 525, 335, arXiv:2307.09041
- Zhang, X. G., 2023c, *ApJS*, 267, 36
- Zhang, X. G., 2025, *ApJ*, 979, 147, arXiv:2412.15506
- Zheng, Z.; Butler, N. R.; Shen, Y.; et al., 2016, *ApJ*, 827, 56
- Zu, Y.; Kochanek, C. S.; Kozłowski, S.; Udalski, A., 2013, *ApJ*, 765, 106
- Zu, Y.; Kochanek, C. S.; Kozłowski, S.; Peterson, B. M., 2016, *ApJ*, 819, 122